Chromosome disentanglement driven via optimal compaction of loop-extruded brush structures

Sumitabha Brahmachari[1, *] and John F. Marko[1, 2]

[1]*Department of Physics and Astronomy, Northwestern University, Evanston, IL 60208*
[2]*Department of Molecular Biosciences, Northwestern University, Evanston, IL 60208*

Eukaryote cell division features cyclical manipulation of the compaction state of chromosomes that is synchronized with their physical and topological segregation. It has been proposed that lengthwise compaction of chromatin into mitotic chromosomes via loop extrusion underlies the compaction-segregation/resolution process. We analyze this disentanglement scheme via considering the chromosome to be a succession of DNA/chromatin loops - a polymer "brush" - where active extrusion of loops controls the brush structure. Given topoisomerase (TopoII)-catalyzed topology fluctuations, we find that inter-chromosome entanglements are minimized for a certain "optimal" loop size dependent on the average chromosome size in accord with experimental data, suggesting that selective pressure has pushed chromosome architecture to one with minimal entanglement. Application of the model to the interphase genome indicates that active loop extrusion can maintain a level of chromosome compaction with suppressed entanglements; the transition to the metaphase state ramps up lengthwise compaction, driving complete topological segregation. Optimized genomic loops may provide a means for evolutionary propagation of gene-expression patterns while simultaneously maintaining a disentangled genome. We also find that compact metaphase chromosomes have a densely packed core along their cylindrical axes that explains their observed mechanical stiffness. Our model proposes a unified view of structural reorganization of chromosomes through the cell cycle in good agreement with a wide range of experimental observations for varied organisms, predicts testable scaling laws including the long-known relationship between genome size and metaphase chromosome thickness, and can be generalized to the case of bacteria.

---

* Electronic address: sumitabha@u.northwestern.edu; current address of this author is at the *Center for Theoretical Biological Physics, Rice University, Houston, TX 77005*

I.   INTRODUCTION

Chromosomes are long biopolymers residing in confined spaces. For eukaryotes, the nucleus is the confining compartment, while bacterial chromosomes are confined by the cell itself. The fraction of the total confinement volume occupied by all the genomic segments, i.e., the average volume fraction of the genome, is high enough to force strong overlap between different chromosomes [1]. Active manipulation of the topology of chromosomes is essential for their disentanglement and segregation as occurs during cell division. Type-II DNA topoisomerases (Topo II) catalyze the passage of one genomic segment through another, driving a unit change in inter-chromosome linkage, and are essential enzymes for chromosome disentanglement. However, individual Topo IIs are unable to sense the net inter-chromosomal topology, and by themselves cannot drive chromosome disentanglement [2–4].

Eukaryote chromosomes also undergo significant and highly ordered compaction during mitosis. This process cannot be "condensation" in the usual sense of that term: uncontrolled self-adhesion of chromatin will lead to a compact and highly entangled genomic globule. Instead, chromosome segregation must be based on "lengthwise compaction" simultaneous with Topo II-mediated topology changes, cooperating to drive progressive physical and topological segregation [5, 6]. Processive extrusion of genomic loops by loop-extruding enzymes has been proposed to underlie lengthwise compaction [7, 8] and the formation of the long-observed cylindrical brush (loop array) structure of metaphase chromosomes [9–11]. The "loop-extrusion" hypothesis proposes a microscopic mechanism to achieve lengthwise compaction of chromosomes based on molecular-motor-generated tension along the polymer contour [7, 8]. In other models of chromosome compaction, such a compaction-generating tension may be effectively generated by mechanisms like supercoiling flux arising from transcription and replication [12], or "sliding" of genomic contacts driven by directed motion of molecular slip-links [13, 14], or diffusion of genomic segments in a hypothesized data-driven potential [15, 16].

Structural Maintenance of Chromosomes (SMC) complexes are thought to be responsible for organizing chromosome structure [17–25], and recently have been directly observed to processively translocate and loop-extrude DNA[26, 27]. The three-dimensional conformation of the interphase genome has been observed to be organized into loops that regulate gene expression, and these loops appear to be actively driven by a concerted action of SMC complexes and architectural proteins [20, 24, 25, 28–33]. Electron microscope images of metaphase chromosomes have directly observed the loop organization of metaphase chromosomes, supporting a polymer brush model featuring radially emanating loops [9, 10, 34].

Here, we show that loop-extruding motors capable of exerting ≈ 1 piconewton (pN) force are sufficient to drive compaction to a stage where osmotic repulsion between chromosomes will lead to a steady-state of disentangled chromosomes, given that entanglement topology is allowed to change (Topo II is active). Compaction tension generates stress in chromosomes, which is then relaxed through entanglement release by Topo II: the coupling of compaction to topological simplification provides the key driving force directing Topo II to disentangle the genome. While simulations of loop extrusion in a fluctuating-topology ensemble have indicated that the coupling of loop extrusion to lengthwise compaction is a feasible mechanism to drive topological simplification[35], a scaling theory with predictive results for a wide range of genome and chromosome sizes is lacking.

To address this, we develop a cylindrical polymer brush model of chromosomes that reveals how active manipulation of the brush structure via loop extrusion can drive genomic disentanglement. We find that for given genome size, average chromosome size, and confinement volume fraction, there is an optimal loop or "bristle" size that simultaneously maximizes lengthwise compaction and minimizes inter-chromosome entanglement. Qualitatively, this occurs since for small loops, chromosomes have a long axial length and easily become highly entangled. As the loops grow in size, the chromosome is gradually lengthwise-compacted to become a cylindrical brush of size smaller than the original chromosome [Eq. 2], and entanglements between chromosomes are reduced. If the loops become so large that they are comparable to the size of the chromosomes themselves, the chromosome becomes a "star polymer" with long bristles which once again become highly entangled with bristles of neighbor chromosomes [Fig. 1(d)]. Experimentally observed genomic loops are quantitatively similar in size to this predicted optimal loop size, suggesting that organization of the genome into loops of specific, regulated size is important to maintaining a low level of genomic entanglement. While we will discuss our results primarily in the context of eukaryotes, we also show how they can be applied to bacterial chromosomes.

II.   POLYMER MODEL AND METHODS

a.   ***Chromosomes are polymers of nucleosome monomers.***   We consider chromatin as a self-avoiding polymer made up of nucleosome monomers of diameter $a \approx 10$ nanometers (nm), such that the blob size or the Flory
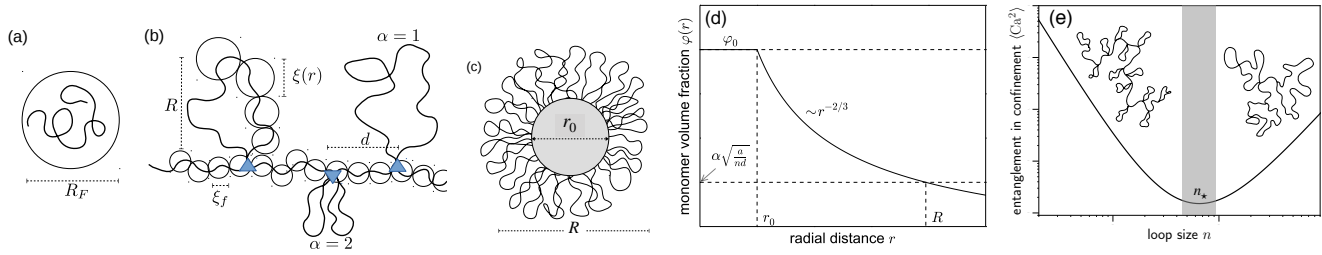
FIG. 1. (a) Flory radius or equilibrium dimension of self-avoiding polymer [Eq. 1]. (b) Sketch of loop-extruded chromosome showing chromatin loops along backbone, where circles represent the correlation length ξ. Out of the three schematic loops sketched, the middle one is divalent ($\alpha = 2$) and the other two are monovalent ($\alpha = 1$). (c) Cross-sectional view of compacted chromosome. Circular cross-section corresponding to the gray-shaded area is the densely-packed-chromatin core of width r_0. (d) Monomer volume fraction $\varphi(r)$ is maximum inside the core [$\varphi_0 \approx 1$] and decays radially outwards. (e) Inter-chromosome entanglements per chromosome $\langle Ca^2 \rangle$ [(3)] as a function of loop size for genome size N, given backbone size m, and a fixed nuclear volume shows a minimum for an optimal configuration with loop size $n_\star$, shown by a shaded region. This follows from the finite size of chromosomes. Schematic pictures of finite-size chromosomes in the small- and large-loop regimes are shown.

radius of a chromosome of N nucleosomes is given by [1],

$$R_F(N) = aN^{3/5} \tag{1}$$

Eq. 1 assumes good solvent conditions, corresponding to complete mutual exclusion among nucleosomes without self-adhesion. We denote the total number of monomers (nucleosomes, each containing roughly 200 bp) in the genome by $\mathcal{G}$, and the number of chromosomes of a cell by k (karyotype), so that $N = \mathcal{G}/k$, is the chromosome size, or average number of monomers in a chromosome. The contour length of a completely unfolded chromosome (chromatin) is $L = Na$.

    b. ***Cylindrical polymer brush chromosomes.*** We model chromosomes as a succession of chromatin loops connected by a chromatin backbone [Fig. 1(b); in the bacterial case the polymer is DNA coated by nucleoid-associated proteins with a similar value of a but containing fewer base pairs, see below]. The resulting cylindrical bottlebrush polymer has three independent, active structural parameters: *loop size n*, the average number of nucleosome monomers per loop; *backbone size m*, the average number of nucleosome monomers between adjacent loop anchors; and *loop valency α*, the degree of subdivision (branching) of larger loops into smaller ones. A loop of size n with a valency α indicates there are α subloops each of size n/α associated with the same anchoring location [Fig. 1(b)]. As an example, human metaphase chromosomes are thought to have $n/\alpha \approx 500$ (≈ 100 kb) [25].

    When the backbone is longer than the loops ($m > n$), adjacent loops do not overlap and the brush approaches the self-avoiding "random coil" limit [Eq. 1]. Alternately, when $m < n$, there is a stretching tension along the backbone from overlap of adjacent loops that generates a stiffening response, pushing the structure towards the densely-grafted "polymer brush" limit.

    A key physical parameter for the brush is the *interloop distance d*, the spatial distance between adjacent loop anchors: d is the steady-state end-to-end extension of the backbone segment of m monomers. A polymer brush morphology requires $d < R_F(n)$ and $d > R_F(m)$. The value of d is set by a force balance between the osmotic repulsion of adjacent loops: $f \approx k_B T a^{5/8} n^{3/8} d^{-13/8}$, that drives an increase in d, and the entropic elasticity of the backbone which favors a decrease in d, since $d > R_F(m)$. This force balance gives $d = an^{3/25}m^{12/25}$, which is valid until the stretching force reaches a critical value: $f_\star = k_B T/a \approx 0.4$ pN, corresponding to a completely stretched backbone, whereupon the interloop distance becomes linear with backbone size. This transition occurs when the backbone size is a small fraction of the loop size, $m_\star = n^{3/13}$ [36].

    The backbone tension is a result of the osmotic stress generated from a high volume fraction of monomers near the backbone. As is typical for a cylindrical polymer brush, the monomer volume fraction decreases radially outwards causing an osmotic pressure gradient that radially stretches the loops: $R \sim n^{3/4}d^{-1/4}$, and establishes a long thermal bending persistence length: $\rho \sim n^{15/8}d^{-17/8}$, reflecting a stiffening response [34, 36–38]. The average monomer volume fraction is higher for lower interloop distance and higher loop branching: $\varphi \sim \alpha^{2/3}d^{-2/3}$. This generates a region along the backbone of the brush, we refer to as the "core", that features dense packing of the monomers ($\varphi_{core} \approx 1$) and a high osmotic pressure [Fig. 1(c-d)]. The width of the core is proportional to the loop valency and inversely proportional to the interloop distance: $r_0 \approx \alpha a^2/d$. This relation, derived from the geometric condition that the surface of the core form a surface saturated by "grafted" loops, indicates that more closely packed loops and loops with higher branching generate a thicker core. We note that while the existence of maximal-density core has been

long discussed in connection with spherical polymer "micelles" [39], the cylindrical polymer brush literature has not recognized this possibility, which appears to be key to understanding chromosome folding.

The axial contour length of brush chromosomes has a non-monotonic dependence on loop size due to the finite-size end loops that dominate in the large-loop "star polymer" limit (i.e., when the whole chromosome is "end"):

$$L' \approx Nd/n + R_F(n) \tag{2}$$

The first term corresponds to the cylindrical part of the brush where each loop contributes d to axial length; the second term is from the end loops that are less confined than their counterparts in the middle of the brush. Note, Eq. 2 corresponds to the brush limit of the chromosomes, where $n + m \approx n$. Minimization of the extension gives an *optimal loop* size: $n_\star = m^{12/37} N^{25/37}$. An *optimal brush* is a tandem arrangement of optimal loops that has two independent parameters: m and α, where the loop size is imposed by minimization, which, as we discuss next, also minimizes inter-chromosomal entanglements.

   c. **Entanglement between chromosomes in a confined volume.** We measure entanglement between chromosomes confined within a volume from the number of inter-chromosomal concentration blob collisions [5], under conditions where entanglement topology can freely fluctuate (in the presence of Topo II). The number of such collisions between polymers in a semidilute solution scales linearly with the number of polymer segments: $\langle Ca^2 \rangle_0 \approx N\phi^{5/4}/N_e$ [5], where ϕ is the average volume fraction of the confined genome and $N_e \approx 100$ is the entanglement length [5, 40]. The number of collisions between segments of the brush and therefore |Ca| are much lower due to the smaller number of statistical segments N':

$$\frac{\langle Ca^2 \rangle}{\langle Ca^2 \rangle_0} \approx \left(\frac{R_F(N')}{R_F(N)} \right)^{15/4} = \left(\frac{L'}{R_F(N)} \right)^{15/4} = \left(\frac{m}{N} \right)^{27/37} \tag{3}$$

where the last two equalities follow for optimal brushes.

   Since $N' \approx L'/\rho \approx (m/N)^{51/74} < 1$ there is a strong suppression of entanglement level in a solution of optimal brushes, denoted by $\langle Ca^2 \rangle$. The entanglements between brushes are therefore minimized for optimal loops and the level of entanglement can be reduced by shortening the backbone of the optimal brush (for calculation details see Appendix A). Throughout, we assume a fluctuating topology ensemble, i.e., that Topo II allows topological equilibration for a given chromosome loop structure. Topology fluctuations ensure local entanglements do not hinder structural reorganization, and avoid the slow reptation dynamics of usual entangled polymers [1].

III.   RESULTS

   a. **Optimal loops maintain a basal level of chromosome compaction and suppress inter-chromosomal entanglements in nuclear confinement.** Optimal loop size minimizes chromosome axial length L' [Eq. 2]. The existence of the optimal state arises from the fact that when the loops are small, there are a large number of them, each contributing about one interloop distance d to L'. On the other hand, if the loops become so large that the equilibrium unperturbed size of the loops at the end of the cylindrical brush begins to dominate, L' is again large. A loop size between these limits minimizes L'.

   Figure 2 shows the optimal subloop size, which is obtained by dividing the optimal size by the valency or the number of loop branches. An optimal loop $n_\star$ with valency α indicates there are α subloops, each of average size $n_\star/\alpha$ emanating from the same anchoring location. Optimal loops with higher valency have smaller subloops.

   In terms of inter-loop-anchor "backbone" segment size m, optimal loops are larger for a brush with larger m (Fig. 2) since longer end loops are needed to compete with the larger contribution to L' from the longer backbone; increasing m eventually leads to formation of a random-coil polymer. Making the backbone small leads to the limiting size $m_\star$, where the tension from overlap of closely anchored loops completely stretches the backbone, and where interloop distance is linear with backbone size: $d \sim m_\star \sim N^{15/89}$ [Table I]. The optimal brush with a fully stretched backbone has the minimum axial length L', associated with an axial stretching tension $f_\star = k_B T/a \approx 0.4$ pN.

   The different lines in Fig. 2 correspond to values of m and α that represent different overall conformations of the brush chromosomes. The blue dashed line ($m = 10^3$ and $\alpha = 1$) corresponds to a "sparsely grafted" configuration of monovalent loops, such that overlap between adjacent loops minimally stretches the backbone. The orange dashed line ($m = 10^3$ and $\alpha = 50$) corresponds to a sparse configuration of branched loops. The green solid line ($m = m_\star$ and $\alpha = 1$) corresponds to a "dense" regime of brush where the adjacent monovalent loops are closely grafted, such that the strong repulsion between them leads to a highly stretched backbone and a stiff polymer brush. The red solid line ($m = m_\star$ and $\alpha = 50$) is for a dense brush featuring high degree of loop branching. Finally, the purple dot-dashed
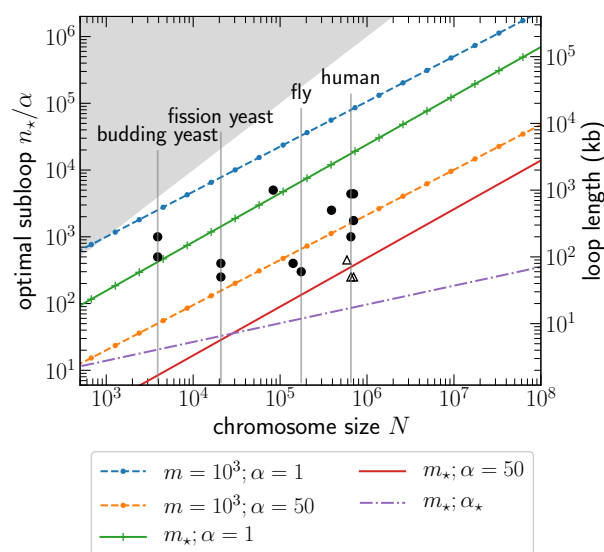
FIG. 2. Optimal loops of size $n_\star$ minimize axial length of the brush chromosome and suppress chromosomal entanglements. Loop size divided by valency α (number of branches), gives the size of subloops, plotted versus the total number of chromosomal units N. Curves correspond to different number of monomers in the backbone segment between two consecutive loops m and valency α. Optimal loops are larger for larger m. A fully stretched backbone, owing to the tension generated from overlapping adjacent loops, corresponds to $m = m_\star$ [Table I], the minimum size of the backbone for an optimal loop. Higher valency α leads to smaller subloops due to increased loop branching and increases the density of the monomers in the interior of the brush. Valency $\alpha_\star$ scales with N, and corresponds to a phenomenological value for metaphase chromosomes [Table I]. Gray-shaded region is inaccessible, as it corresponds to a loop size greater than the chromosome length. Filled circles are experimental data for "loop domains" in the interphase genome obtained from chromosome contact or Hi-C maps [28–30, 32, 33]; open triangles denote loops identified from electron-microscope images of metaphase chromosomes [9, 10]. The data indicate that an entanglement-suppressing optimal loop size is maintained throughout the cell cycle: during interphase, the loops have a lower valency and are less compact, whereas during mitosis, the loops are heavily branched, leading to smaller subloops. The experimental data also respect the physical limits imposed by our tandem-loop model. The y-axis on the right shows the loop lengths in kilobase pair (kb) units.

line ($m = m_\star$ and $\alpha = \alpha_\star$) corresponds to a dense, stiff brush with highly branched loops – a model for compact metaphase chromosomes; the degree of branching $\alpha_\star$, which scales with N (see below and Table I), is determined from the elastic modulus of metaphase chromosomes [41].

Hi-C experiments studying the three-dimensional conformation of the less-compact interphase genome find a characteristic loop size [28–33] (Fig. 2, filled circles). Fig. 2 suggests that these interphase chromosome loops maintain a brush-like structure of the chromosome, driving a level of compaction quantitatively similar to optimal loops. Our results suggest that average loop size n/α may have been influenced by the fact that they minimize L' and reduce inter-chromosomal entanglements [see below and Fig. 3], facilitating a finer control over gene regulation via *cis* contacts.

Loop sizes obtained from electron-microscope images of metaphase chromosomes [9, 10], which are somewhat smaller than interphase loops (Fig. 2, open triangles). Increasing interphase loop valency is a conceivable way to drive mitotic chromosome compaction, but Hi-C experiments do not indicate any sequence-specificity during mitosis [25, 31], suggesting a major refolding of the genome that is stochastic in nature. DNA replication may be responsible for partial loop disassembly, but the brush morphology is likely not entirely disassembled since that would lead to a high degree of interchromosome entanglement [Fig. 3]. Continuous chromatin-loop-extruding SMC complex activity is likely necessary to maintain polymer-brush structure and the associated level of compaction in interphase; a higher level of loop-extrusion activity can then drive the formation of dense brush-like mitotic chromosomes. The presence of loops and loop-extruding complexes throughout the cell cycle is likely important to avoid chromosome entanglement (see Discussion).

b. ***Chromosomes can be completely disentangled via compacting optimal loops.*** Optimal brush chromosomes are semiflexible polymers, since the overlap between adjacent loops leading to the stretching tension along backbone generates a stiff response to bending, and the brush has a thermal persistence length comparable to its axial length. The lower number of statistical segments of the optimal brush than that of the constituting chromatin leads
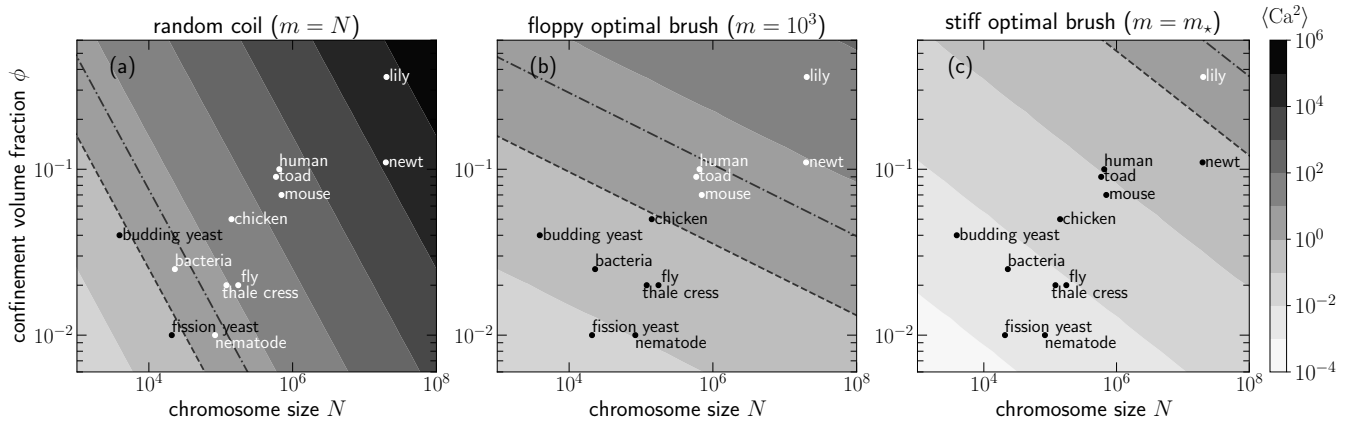
FIG. 3. Removal of inter-chromosomal entanglements by establishing an optimal brush configuration via loop extrusion in the presence of topology fluctuations. A cell with a given nucleus volume, number of chromosomes, and an average chromosome size N occupies a specific position in the above (N, ϕ) diagram, where ϕ is the net volume fraction of all the chromosomes within nuclear confinement. Shading indicates level of entanglement $\langle \text{Ca}^2 \rangle$ [Eq. 3], where a lighter (darker) shade depicts a lower (higher) entanglement or inter-chromosomal contacts per chromosome (see legend to the right). Dashed line shows $\langle \text{Ca}^2 \rangle = 1$ in the nucleus: above this line cellular chromosomes are entangled ($\langle \text{Ca}^2 \rangle > 1$), while a cell lying below the dashed line has a disentangled genome ($\langle \text{Ca}^2 \rangle < 1$). Dot-dashed line shows $\langle \text{Ca}^2 \rangle = 1$ line after nuclear envelope breakdown (NEB), where the confinement volume is increased 3-fold over that of the nucleus; NEB mildly aids chromosome disentanglement. (a) Chromosomes considered as random coils of self-avoiding polymers exhibit a significant degree of entanglement ($\langle \text{Ca}^2 \rangle_0 \sim N\phi^{5/4}$), that increases with the chromosome size. Notably, yeast chromosomes are essentially disentangled in the random coil state. (b-c) Chromosomes modeled as polymer brushes are more compact and as a result are less entangled. Entanglements between chromosomes can be reduced by organizing the chromosomes into a tandem array of optimal loops, which have a minimal end-to-end extension for a given backbone segment size m. Contour plots show that in steady state optimal brush chromosomes have a lower entanglement level than the random coil state. Further removal of entanglements is possible by stiffening the optimal brush via stretching and shortening the backbone. Interphase chromosomes have larger loops separated by long backbone segments, making them less compact, floppy brushes that are also less entangled than a random coil. Loop extrusion mechanism can modulate the brush configuration to generate an order $k_B T/a \approx 0.4$ pN stretching tension along the backbone, ultimately leading to stiffening and complete disentanglement of chromosomes.

to a lower level of entanglement between brush chromosomes [Eq. 3].

The equilibrated-topology entanglement level $\langle \text{Ca}^2 \rangle$ [Eq. 3] may be estimated as proportional to the number of inter-chromosomal contacts per chromosome; each contact represents a point where a crossing between two genomic segments can be reversed in sign without significant perturbation of chromosome conformation [6]. Unfolded chromosomes generally show a high degree of inter-chromosomal entanglement [Fig. 3(a)], since the scale of nuclear confinement is smaller than the unperturbed equilibrium random-coil size of unlooped chromosomes [Eq. 1] [1]. The increased confinement volume upon nuclear envelope breakdown (NEB) is a mild effect, and by itself, does not strongly drive segregation of chromosomes [Fig. 3(a)]. Interestingly, nematodes and yeast have essentially disentangled genomes even in a random-coil state, indicating that segregation of chromosomes is a less pressing concern for these organisms compared to, e.g., mammals, whose chromosomes can get highly entangled. Some lower eukarya (e.g., budding yeast) are known to *not* have NEB during mitosis, i.e., "closed" mitosis [42]; the essentially disentangled genome inside the nucleus of these organisms may have contributed to this evolutionary outcome.

The entanglement level is much lower (for given confinement volume fraction and chromosome size) when the chromosomes are organized as a tandem array of optimal loops [Fig. 3(b)], highlighting the importance of loops during interphase. Figure 3(b) is plotted for $m = 10^3$, a regime in which the optimal brush is relatively "floppy", i.e., the backbone size is smaller than that required for an overlap between adjacent optimal loops ($m < n_\star$), but larger than that for which the backbone is completely stretched and stiff ($m > m_\star$, see Table I). Figure 3(a) shows the maximum possible entanglement between chromosomes for a given confinement volume fraction and average chromosome size: due to interphase looping, chromosomes are never strongly entangled.

Reducing backbone size (lower m) reduces the level of inter-chromosomal entanglements, reaching a minimum value for a completely stretched backbone [$m = m_\star$, see Fig. 3(c)]. Stretching and shortening the backbone leads to a stiffening response of the optimal brush that drives the disentangled state. Given typical nuclear volume fractions, stretching the backbone of optimal brush chromosomes (force ≈ 1 pN) completely disentangles them.

TABLE I. Example values of the minimum backbone size: $m_\star = N^{15/89}$, and metaphase valency: $\alpha_\star = (0.5)N^{40/89}$

organism	chromosome size (N)	minimum backbone size ($m_\star$)	metaphase valency ($\alpha_\star$)
budding yeast	4×10^3	5	20
human	6.5×10^5	10	200
newt	2×10^7	20	1000

*c.   **Compact chromosomes have a dense axial core featuring closely packed monomers that impart mechanical rigidity.***   Compaction of the optimal brush chromosomes can be controlled via two physical processes: one, shortening the backbone, i.e., shorten m; and two, increasing the valency of the optimal loops α. Both these processes increase the monomer concentration in the interior of the brush, leading to an overall compaction; however, the signatures of these processes on the compacted structure are different: shortening the backbone compacts the axial length [Eq. 2], while, increasing the average valency of optimal loops compacts the lateral dimension or thickness of the chromosomes: $R \sim \alpha^{-1/2}$.

Higher monomer concentration inside the brush leads to a densely packed core where the monomer volume fraction is near maximal (≈ 1), and consequently, the core has a high osmotic pressure $\approx k_B T/a^3 \approx 4$ kilopascals (kPa). This contrasts with the much smaller bulk modulus for an ordinary (uncrosslinked) semidilute polymer solution ≈ 10 Pa, due to alower volume fraction ≈ 0.1.   The elastic modulus of brush chromosomes shows a strong dependence on the average loop valency: $E \sim \alpha^{9/4}$. We can use the experimental value of metaphase chromosome elastic modulus $E_{\mathrm{meta}} \approx 1$ kPa [41, 43, 44] to more precisely determine the *metaphase loop valency* for an optimal brush with fully stretched backbone: $\alpha_\star \approx cN^{40/89}$. Here $c = (E_{\mathrm{meta}} a^3/k_B T)^{4/9} \approx 0.5$ is an order-unity constant [Table I].

Figure 4(a-c) show the structural aspects of the brush chromosomes for various m and α. Comparison with metaphase data suggests that metaphase chromosomes have a sufficiently stretched backbone ($m = m_\star$) supporting highly branched loops ($\alpha \gg 1$). The curves for metaphase valency ($\alpha_\star$) agree well with experimental observation, indicating that metaphase chromosomes have dense chromatin cores that are about hundred nm thick [Fig. 4(d)]. Stabilization of the core requires compaction pressure to compensate osmotic repulsion between monomers inside the core; loop-extruding SMC complexes and other cross-linking proteins are crucial to generate this compaction pressure.

The thermal bending persistence length, and the doubling force are measures of mechanical rigidity, and show strengthening of the brush in metaphase due to formation of the thick core [Fig. 4(e-f)]. The doubling force, the force associated with linear stretching of the chromosome to twice its native length, is $f_0 = (\partial^2 F/\partial d^2)d \sim \alpha^{5/4}$, where F is the free energy per loop (see Appendix A).

*d.   **Bacterial chromosomes.***   Bacteria, unlike eukaryotes, do not have nucleosomes; instead, bacterial DNA inside cells is coated with a variety of nucleoid-associated proteins (NAPs), e.g., HU, H-NS and IHF [45]. Like eukaryotes, bacteria possess SMC proteins (in *E. coli*, MukBEF [46]) and bacterial versions of eukaryote TopoII. We treat bacterial chromosomes as self-avoiding polymers, with cylindrical monomer units of length $a \approx 50$ nm (comparable to the persistence length of naked DNA [47]) and width $b \approx 5$ nm, corresponding to the thickness of protein-bound DNA segments (NAPs can reduce the persistence length but this is not crucial here). This gives a monomer aspect ratio parameter $\lambda = a/b \approx 10$; however, the structure optimization discussed above for symmetric nucleosome monomers in eukaryotes does not depend on λ (see Appendix A), making the previously discussed results directly applicable to bacterial chromosomes.

The bacterial genome has the potential to be appreciably entangled due to its substantial confinement [Fig. 3(a)], highlighting the need to drive compaction in order to segregate multiple copies. However, only mild compaction compared to higher eukaryotes is required [Fig. 3(b)]. Bacterial DNA is also subject to a global supercoiling pressure, by virtue of DNA gyrase, a motor-like enzyme that maintains bacterial DNA in a supercoiled condition. Supercoiling may play an important role in driving compaction and maintaining an optimal brush conformation of bacterial chromosomes. The restoring force of a plectonemic domain for physiological levels of bacterial supercoiling ≈ 0.5 pN [48], can generate the stretching tension along the backbone connecting plectonemic domains, necessary to drive compaction and segregation of bacterial chromosomes. This is in accord with models of bacterial chromosome organization into territories driven by DNA supercoiling [12].

For elongated bacterial cells that are asymmetric (e.g., *E. coli* and *C. crescentus*), there will be an entropic-segregation pressure gradient along the long axis of the cell. This pressure gradient may aid chromosome segregation by pushing the two sister chromosomes to opposite poles of the long axis [49]. The cylindrical brush structure of chromosomes, driven by loop extrusion, enhances this pressure gradient, and provides an active mechanism to control segregation. Other mechanisms may work in parallel: some bacterial species possess chromosome tethering mechanisms that may aid in driving axial segregation [50].
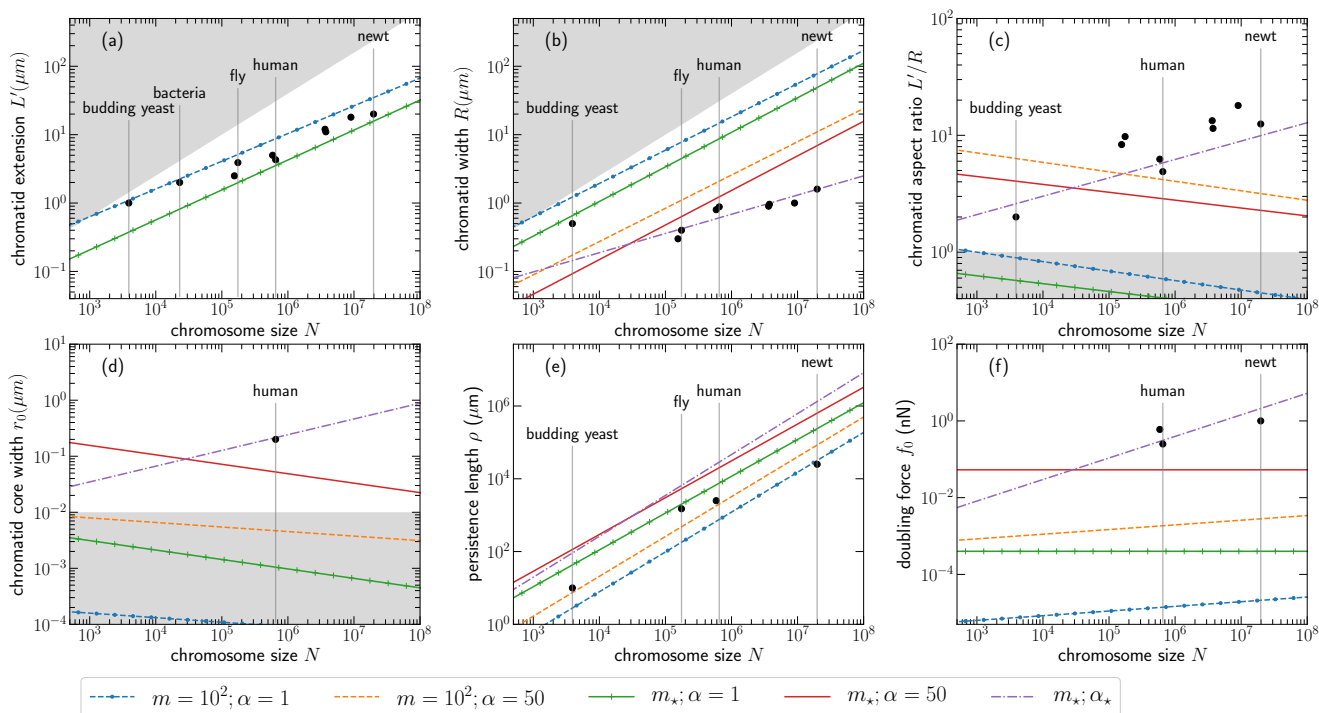
FIG. 4. Structure and mechanics of compact mitotic chromosomes result from the densely-packed chromatin core. Filled circles show experimental values for metaphase chromosomes [see Appendix A]. For the bacterial case, filled circle shows the dimension of a cellular chromosome which compares with the cellular dimensions. Lines correspond to the cases described for Fig. 2. (a) Average chromatid axial length L', (b) chromatid width R, and (c) length-to-width aspect ratio (L'/R) show that the change in width is stronger upon stiffening the brush via shortening the backbone (lower m) and increasing the loop valency (higher α). Larger valency values promote a higher monomer concentration in the interior of the brush and generate a core where the monomers are densely packed. The core enhances the mechanical rigidity of the chromosomes; the width of the core r_0, which is proportional to the average loop valency, is plotted in (d); the lines lying in the shaded region in (d) do not have a core, since a minimal core must be at least one monomer thick. The experimental data for human chromosome core corresponds to the thickness of the axial region where condensin-colocalizes in metaphase [23]. The thermal persistence length of the brush ρ (e), and the force associated with stretching the chromosome to twice its native length or the doubling force f_0 (e), show increased stiffness and mechanical rigidity for smaller backbone and higher valency. The valency $\alpha_\star$, which is required to reproduce the observed metaphase-chromosome elastic modulus ≈ 1 kPa and is $\approx 40\%$ of the maximum allowed valency of an optimal loop, agrees well with metaphase chromosome size data. This indicates that the dense core resulting from backbone stretching and branching of chromosomal loops, achievable via a loop extrusion mechanism, can underlie the emergent mechanical rigidity and compactness of metaphase chromosomes. Shaded region in (a) and (b) correspond to chromosome for which the backbone is comparable to the loop size leading to no overlap between adjacent loops, which approaches the random coil limit of the polymer brush: $L' \approx R_F(N)$ and $R \approx R_F(N)$. This suggests bacterial chromosomes are only minimally compacted in the axial dimension. Also, note that backbone segments with $m = 1000$ monomers correspond to overlapping adjacent optimal loops for all relevant chromosome sizes.

The optimal loop result for the *E. coli* nucleoid of axial length 2 μm corresponds to a floppy brush (blue dashed line in Fig. 4(a)), which permits full segregation but with enough flexibility to allow the nucleoid to be folded and moved around inside the cell. The bacterial nucleoid is heavily confined, evident from the large expansion (3 to 10 fold linear dimension) of the bacterial chromosome following cell lysis. Bacterial nucleoids removed from cells behave as polymer networks of roughly $10 - 20$ μm maximum extension, [50, 51], consistent with the maximum extension of a loosely compacted brush of axial length ≈ 2 μm.

IV. DISCUSSION

a. ***Optimal loops compact chromosomes and suppress inter-chromosome entanglements.*** Eukaryote chromosomes appear to be organized into loops, as long directly observed for the mitotic case by electron microscopy [9, 10], and established more recently for interphase genomes [28–30, 32, 33]. We have shown that folding a chro-

mosome in loops of a chromosome-size-dependent length $n_\star$, simultaneously maximizes compaction and minimizes interchromosome entanglements [Figs. 2 and 3]. These optimal loops or subloops formed upon branching are comparable to experimentally observed loops through the cell cycle, suggesting a role of chromosomal loops in suppressing entanglements, both during interphase and mitosis. These loops keep the chromosomes territorialized throughout the cell cycle, tightly regulating interchromosome entanglement. Larger loops and a longer backbone allow a controlled level of entanglement in interphase, which is essential for gene expression. While the positioning of these loops affect transcriptional regulation, correspondence of their sizes to that of entanglement-suppressing optimal loops is plausibly a result of evolutionary selection.

On the other hand, compact mitotic chromosomes have short, stretched backbones ($m = m_\star$) with heavily branched loops ($\alpha \gg 1$), that efficiently remove all the entanglements between chromosomes leading to their segregation [Fig. 3]. The predicted size of mitotic subloops required to reproduce the experimentally observed chromosome stiffness is smaller than the subloops observed in Electron-microscope images [Fig. 2]. A larger subloop in our model will lead to a lower chromosome stiffness moduli, however, the mechanical rigidity may be compensated by additional crosslinking of chromatin inside the chromosome brush, which we ignore in our simple model.

*b. **Compact mitotic chromosomes have a dense core along their axes.*** Compaction of the tandem array of optimal loops can be achieved by bringing the loops closer at the backbone and/or by increasing the average valency of the loops, i.e., dividing the loop into branches. Both these processes increase the monomer concentration inside the cylindrical brush which generates a core where the monomers are closely packed and there is a high osmotic pressure. The osmotic pressure inside the core enhances the elastic modulus of the brush. Optimal brushes with a fully stretched backbone and a metaphase valency value $\alpha_\star$ [Table I] that is required to reproduce the elastic modulus of metaphase chromosomes ≈ 1 kPa [41, 43, 44], exhibit a dense core that is responsible for the emergent mechanical rigidity of metaphase chromosomes [Fig. 4]. Note, $\alpha_\star$ is $\approx 40\%$ of the maximum allowed valency of an optimal loops, where the maximum valency corresponds to the core filling the entire chromosome.

*c. **Loop extrusion can control the optimal brush structure and thus drive compaction and segregation of chromosomes.*** Active loop extrusion is the likely mechanism driving compaction by controlling loop size n, and backbone size m, thus controlling the interloop distance d [Fig. 1(b)]; extrusion generates interloop repulsion, stretching the backbone segments of chromatin with tension ≈ 1 pN, as compaction occurs. The resulting tightly packed optimal-loop chromosome itself behaves as a semiflexible polymer, exhibiting self-avoidance at the chromosome scale.

Proteins of the family Structural Maintenance of Chromosomes (SMC complexes: cohesin and condensins) are prime candidates for active loop-extruding elements [19, 22, 52], have been directly observed to translocate on and loop-extrude DNA at the single-molecule level [24, 26, 27], and can compact DNA against forces of up to ≈ 1 pN [53–57]. The ubiquitous presence of DNA-bound SMC complexes in all cells can ensure stretching of backbone segments, important for maintaining a semiflexible chromosome brush, and consequently a low entanglement level between confined chromosomes throughout the cell cycle. The stochasticity of loop extrusion process, which can be controlled *in vivo* by directly controlling the concentration the loop-extruding enzymes and/or via controlling the activity of the SMC complexes (e.g., by altering the residency time of the SMC complexes on DNA [20]), is important in maintaining an average loop size [8]. This allows an entanglement-suppressing optimal configuration of chromosomes in the cellular environment where formation of transient genomic contacts is an essential feature.

*d. **Loop extrusion is essential to maintain the optimal structure during interphase.*** The size of the interphase loops and their positioning depends on proper functioning of the loop-extruding SMC complexes: loops may either get disassembled or attain an increased stability upon impairing the normal activity of SMC complexes. Destabilization of interphase loops, triggered by the removal of cohesin or condensin is expected to disrupt the optimal structure, resulting in higher chromosomal overlap, i.e., loss of chromosomal territories [22], and a concomitant increase in the inter-chromosomal entanglements.

On the other hand, increased stability of interphase loops, driven by a higher residency time of cohesin on the chromosomes, leads to a compact string-like "vermicelli" phenotype of interphase chromosomes [20]. A phenotypically similar situation of interphase chromosome compaction, called "premature chromosome condensation" (PCC), occurs upon fusion of interphase and mitotic cells [58, 59]. Compaction of interphase chromosomes in these cases is likely associated with increased loop extrusion activity that results in a stretched backbone and highly branched loops, promoted by either increased activity of interphase SMC complexes or introduction of mitotic-specific SMC complexes.

Various non-SMC complexes, that may or may not interact with the SMCs, are also relevant to maintaining the optimal structure. The structural protein CTCF that is known to interact with SMCs, has been found to reinforce certain loops that are important for gene regulation [32]. Some of these CTCF-mediated loops have been reported to

remain stably bound throughout the cell cycle [60, 61], which may be associated with propagating a structural template that stores a pattern of gene expression while simultaneously minimizing chromosomal entanglements. Clustering of genomic elements, like superenhancers or nucleosomes constituted of histones bearing certain chemical marks, provides a possible mechanism to control the valency of optimal loops. Branched configurations of certain loops, stabilized by such clustering or by a cross-talk between the genomic-sequence-independent loop extruders and a sequence-specific DNA-binding protein like CTCF, may efficiently regulate gene expression within the optimal structure. The supercoiling pressure generated from gene transcription may also stabilize certain loops [12].

Compartmentalization of the genome into early- and late-replicating domains [28], where the early replicating domains tend to house the highly-transcribed genes, may provide means to implement varied levels of loop extrusion within the interphase genome. A higher affinity of loop extruders for the highly transcribed regions of the genome or the early-replicating domains can initiate compaction of the replicated sister chromatids before the completion of DNA replication. Replication is expected to cause disassembly of loops, especially when replicating the loop anchoring regions; however, disassembly of the entire brush structure leads to entangled chromosomes, a possibility if the loop organization is not reinstated in the replicated regions immediately following their replication.

e. ***Loop extrusion during prophase can drive chromosome disentanglement.*** Strong stretching of the backbone during mitosis, following an increased activity of loop-extruding enzymes leads to stiffening and shortening of the optimal brush chromosomes. This results in their segregation from each other due to osmotic repulsion between the brush segments [Fig. 3(c)] [62]. Reduced cross-talk between loop-extruding machinery and transcription-specific DNA-bound proteins can aid the compaction process, and possibly underlie the observed marked reduction of genomic-sequence-specific loops during mitosis [31]. Condensin II is a likely candidate that drives the prophase compaction, suggesting an important role of condensin II in determining the axial length of chromosomes, in accord with the observation of an increase in the axial length for condensin II-depleted chromosomes [17, 23, 63–65].

The other SMC complex, cohesin is known to hold the sister chromatids during mitosis, however their role in prophase compaction of chromosomes, if any, is not clear. If indeed condensin II is solely driving prophase compaction and segregation, inactivation of cohesin activity in prophase will lead to a factor-of-two increase in the number of chromosomes, which is *not* predicted to be crucially detrimental to their segregation [Fig. 3(c)].

f. ***Topo II-driven topology fluctuations maintain a steady-state topology essential for segregation via compaction.*** Topo IIs allow passage of chromatin segments through one another, permitting chromosome topology to fluctuate. However, Topo IIs cannot disentangle chromosomes by themselves [2–4, 52], since they are unable to directly sense global chromosome topology. By allowing topology fluctuations, Topo II can maintain steady-state topology, allowing disentanglement to occur gradually as lengthwise compaction proceeds. Topology fluctuations mediated by Topo II minimizes stress accumulated at local entanglements that are generated due to reorganization of the brush structure during the course of the cell cycle. Our theory shows that the entanglement level tracks loop extrusion and chromosome architecture. Further work on the time evolution of entanglement release is a next step: DNA tension at interlocks and effective viscosity generated by entanglements are likely to be important.

g. ***Loop extrusion during metaphase can drive structural rigidity via consolidating the core.*** While the axial dimension of a chromosome brush is controlled by loop size and interloop distance [Eq. 2], the brush can be further compacted by increasing loop valency α [Fig. 1(b)], which establishes a dense core along the axes [Fig. 4]. Higher valencies, such as the one corresponding to metaphase chromosomes ($\alpha_\star$), may occur for eukaryote chromosomes via binding of condensin I after nuclear envelope breakdown [25]. The observation that condensin I-depleted chromosomes have a thicker diameter and a lower stiffness [17, 64, 66], supports the notion that these proteins branch loops established by condensin II during prophase, to generate rigid, rod-like metaphase chromosomes with a dense core.

The core supports a high osmotic pressure from the close packing of nucleosomes, and is possibly stabilized by other mechanisms such as mitotic histone modifications that drive nucleosome-nucleosome attraction [67], and a higher concentration of chromatin-crosslinking proteins including Topo II inside the axial core.

h. ***Segregation of sister chromatids from osmotic repulsion between the axial cores.*** Loop extrusion activity on the newly replicated catenated sister chromosomes leads to two brushes that are intertwined near their backbones; the overlapping loops generate a repulsive interchromatid force. The net repulsive force follows from the total osmotic pressure per cross-sectional area of overlap between the two sister chromatids, giving a force acting on each loop of $f_{rep} \approx 10$ pN for monovalent loops, and increases strongly for higher loop valencies $f_{rep} \sim \alpha^{1/2}$ [see Appendix A]. This repulsion drives strand passages by Topo II that will lead to physical segregation of sister-chromosome brushes.

Importantly, an indiscriminate increase of loop valency and crosslinking while the sister-chromatid backbones are still heavily entangled will lead to fusion of the sister chromosomes into a common core, hindering their segregation. This predicts heavily entangled sister chromosomes if condensin I is active inside the nucleus during prophase. Initiation of condensin II compaction and sister chromosome segregation immediately following replication [68, 69], is crucial for timely removal of entanglements *before* establishing a thick core (i.e., before condensin I activity). Once the backbones are disentangled, removal of residual entanglements between sister chromatid loops are facilitated by core formation, since the repulsive force between chromatid backbones is higher for a thicker core. Our model rationalizes the sharp, disjoint compartmentalization of condensin II and condensin I in terms of a kinetic process: establish packed loop arrays first (condensin II) and *then* generate a dense core by loop valency increase (condensin I), and is in line with conclusions drawn from Hi-C analyses [25].

Higher Topo II density along the backbone will speed up the disentanglement dynamics of sister chromosome backbones, and due to its affinity for DNA, Topo II can be expected to preferentially localize to regions of higher DNA concentration, i.e., in the core regions [3, 4, 17]. Fusion of the sister chromatid cores near the centromeric region is unavoidable (the sisters remain attached there until anaphase) High concentrations of Topo IIs and SMCs at the centromere during metaphase, resulting from the high DNA density, will generate strong repulsive forces between the dense and short centromeric loops possibly playing a crucial role in disentanglement of the (peri)centromeric regions [70, 71].

We assume good solvent conditions throughout the article, which is necessary to avoid collapse of all the chromosomes into one genomic globule. However, a multiblock copolymer with deteriorating solvent quality for one of the blocks may be of interest, particularly in interphase. Such a scenario has been suggested as a cause of chromatin compartmentalization via microphase separation [72, 73]. The framework of this paper can be extended to analytically study copolymer and looping degrees of freedom.

In conclusion, we have developed a polymer brush model for chromosomes, where the brush structure is primarily controlled via loop extrusion. Our major result is that the loop organization of the cellular genome is an entanglement-suppressing structure, explaining experimental observations. Lengthwise compaction of the brush results in chromosome segregation, establishing that loop extruders are capable of driving chromosome individualization and chromatid segregation.

ACKNOWLEDGMENTS

Appendix A: Scaling calculations for polymers in the semidilute regime

We adopt the notion of a polymer as a series of non-overlapping deGennes' blobs [1], where the blob size or the correlation length scales inversely with the monomer volume fraction: $\xi = a\varphi^{-3/4}$. And the statistics of the polymer inside a blob is that of a self-avoiding walk or a Flory walk [1, 74]:

$$\xi = R_F(g) = ag^{3/5} \tag{A1}$$

where g is the number of monomers of diameter a in each blob of size ξ.

Throughout this study we assume the topology to be fluctuating, which is a consequence of the presence of TopoII that allows passage of DNA segments through one another at a close-contact site. In such a fluctuating topology ensemble, the number of contacts between chromosome blobs is a measure of entanglement, and disentanglement is possible only when the number of inter-chain contacts is negligible.

1. Cylindrical polymer brush chromosomes

A cylindrical polymer brush has radially increasing blob size, since the net volume accessible to the loops is higher at a larger radial distance resulting in a radially decaying volume fraction.

a. **Radial profile of monomer volume fraction.** Following the arguments originally proposed by Daoud and Cotton [39] for the shpherical symmetry of star polymers, we consider a cylindrical shell of height d, inner radius r, and outer radius $r + \xi(r)$. Since the blobs diffuse radially outward due to the monomer concentration gradient, and there is, on average, α blobs in the considered shell, where α is the loop valency. The volume fraction of monomers in the shell, $\varphi(r)$, is equal to that inside a blob in that shell, leading to the following equations [36]:

$$\varphi(r) = \frac{\alpha g(r)a^3}{rd\xi(r)} = \frac{g(r)a^3}{\xi(r)^3} \quad \Rightarrow \xi(r) = \sqrt{rd/\alpha} \tag{A2}$$

where $g(r)$, the number of monomers per blob of size $\xi(r)$ [Eq. 1].

b. **Osmotic pressure exhibits radial decay.** The osmotic pressure inside the brush Π, scales inversely with the correlation length [1]:

$$\frac{\Pi(r)}{k_B T} = \frac{1}{\xi^3} = \left(\frac{\alpha}{rd}\right)^{3/2} \tag{A3}$$

c. **Loop extension.** The radial extension of a loop, R, containing n monomers can be obtained from radial integration of the volume fraction $\varphi(r)$ [34, 36, 38].

$$\int_0^R dr \; \varphi(r)rd = na^3 \quad \Rightarrow R = \frac{an^{3/4}}{\alpha^{1/2}(d/a)^{1/4}} \tag{A4}$$

The scaling behavior $R \sim n^{3/4}$ resembles a 2D-self avoiding walk, which is a consequence of the effective confinement of a loop in a slit-like geometry due to its neighbors [75].

d. **Loop free energy.** Free energy per loop is given by the number of blobs per loop, because each blob contributes $\approx 1 \; k_B T$ [1]. Equivalently, the free energy per loop may also be obtained from integrating the total osmotic pressure in the cylindrical volume accessible to each loop, as follows [36, 38].

$$\frac{F}{k_B T} = \int_0^R dr \; \Pi rd = \alpha^{5/4} n^{3/8} \left(a/d\right)^{5/8} \tag{A5}$$

e. **Tension along the backbone from loop overlap.** Overlapping loops generates a higher osmotic pressure in the overlap volume that causes repulsion between adjacent loops and leads to a stretching tension along the backbone. We estimate the tension from the free energy per unit length of the backbone.

$$f = -\partial F/\partial d = (k_B T/a)\alpha^{5/4} n^{3/8} \left(a/d\right)^{13/8} \tag{A6}$$

where $f_\star = k_B T/a = 0.4$ pN, is a critical force which completely stretches the entropic degrees of freedom of the backbone chromatin. The correlation length induced by the stretching tension: $\xi_f = k_B T/f$, is at a minimum under the critical force: $\xi_f(f_\star) = a$.

f. **Monomer density along the backbone.** The volume fraction of the monomers along the backbone φ_0, is given by,

$$\varphi_0 = \frac{g_f a^3}{\xi_f^3} = \frac{ma^3}{\xi_f^2 d} \quad \Rightarrow d = ma \left(f/f_\star\right)^{2/3} = am^{12/25} n^{3/25} \tag{A7}$$

where g_f is the number of monomers in a force-induced blob: $\xi_f = ag_f^{3/5}$. The number of monomers per backbone segment between two loops is m and the linear distance between two adjacent loop anchors is d, which we call the interloop distance.. As a simplifying step we consider monovalent loops while computing the steady-state interloop distance from the above force balance between loop repulsion and backbone stretching. Note that d is the extension of the polymer under tension f, which is also called the Pincus regime of polymer extension [76].

To keep our calculations simple, we will employ the limit $n \gg m$, which essentially implies that the chromosomes are always in the "polymer brush" regime where adjacent loops overlap with a varying degree. This contrasts the state where the backbone polymer is long and does not enforce loop overlap ($d > am^{3/5}$), which is similar to the "random coil" or "unextruded" state and corresponds to an ordinary semidilute solution.

g. **Dense axial core.** The monomer volume fraction is maximum: $\varphi_0 \approx 1$, when the correlation length is equal to the monomer size: $\xi_f = a$, which can be established under a critical stretching tension $f_\star = k_B T/a \approx 0.4$ pN. This leads to a densely packed core along the cylindrical backbone. However, the core at this stage is minimally thick $r_0 \approx a$, where r_0 is the radius of the core. The thickness of the core may be increased by increasing the loop valency α.

$$r_0 d = \alpha a^2 \tag{A8}$$

The above relationship between the core radius and loop valency is obtained from the condition that the lateral surface of the right-circular cylindrical core, $\approx r_0 d$, is saturated by the radially emanating α subloops.

Maximum core thickness corresponds to the case where the entire chromosome cross-section forms a compact core, which occurs for a loop valency α_{max}. Using the condition: $(r_0)_{\alpha_{max}} = R$, we get:

$$\alpha_{max} = \sqrt{nd/a} \quad \Rightarrow (r_0)_{\alpha_{max}} = \sqrt{na/d} \tag{A9}$$

h. **Persistence length of brush chromosomes.** A thermally-excited bend generates a curvature κ along the cylindrical brush axes, that has a convex and a concave side. The volume accessible to the loops in the concave (convex) side is smaller (larger) than the unperturbed case by a factor of $\kappa R \ll 1$. This leads to a perturbed volume fraction: $\langle \varphi \rangle (1 \pm \kappa R)$, where the upper/lower signs are for the concave/convex sides respectively, and $\langle \varphi \rangle = na^3/(R^2 d)$ is the average unperturbed volume fraction inside the brush.

The free energy of a loop depends on the average volume fraction as, $F = k_B T n \langle \varphi \rangle^{5/4}$ [Eq. A5]. The perturbation energy due to a curvature κ for a cylindrical brush with persistence length ρ is given by, $k_B T \rho \kappa^2 d$. Hence, we get the persistence length [36, 38]:

$$\rho = n \langle \phi \rangle^{5/4} R^2 / d = a \alpha^{1/4} n^{15/8} (a/d)^{17/8} \tag{A10}$$

The above expression of the brush persistence length can also be consistently derived from the general relation between elastic moduli and persistence length using the following formula [38]: $\rho = R^2 d (\partial^2 F / \partial d^2)$.

Contribution from the core. The core behaves as a solid with an elastic modulus $\approx k_B T/a^3$, and the corresponding persistence length depends on core thickness: $\rho_{core} = r_0^4/a^3$. The core makes the chromosome stiffer, and the net persistence length of chromosomes may be obtained by adding the above contribution from the core to that of the loops. However, in the limit of saturated chromosomes, both the contributions have an identical scaling: $\rho = a(na/d)^2$ [34]. Hence, the contribution from overlapping loops alone sufficiently accounts for chromosome stiffness, and we will employ Eq. A10 for persistence length in our calculations.

i. **Fully stretched backbone for the optimal loop configuration.** Overlap between optimal loops stretch the backbone where the transition to a fully stretched backbone occurs at the critical force value $f_\star$. For optimal loops, this critical repulsive force is obtained when $m_\star = n_\star^{3/13} = N^{15/89}$.

2. Structure and mechanical rigidity of optimal chromosomes

a. **Contour length.** We obtain the axial contour length of cylindrical brush chromosomes with optimal loops and a fully stretched backbone, as follows:

$$[L']_{n_\star} = a m^{36/185} N^{15/37} \tag{A11}$$

b. **Thickness or radial extension.** The average thickness of a chromatid is given by,

$$[R]_{n_\star} = a \frac{m^{21/185}}{\alpha^{1/2}} N^{18/37} \tag{A12}$$

13

c. **Core width.** The diameter of the core scales positively with the level of saturation in the following way.

$$[r_0]_{n_\star} = a\alpha m^{-96/185} N^{-3/37} \tag{A13}$$

d. **Persistence length.** The brush persistence length obtained from Eq. A10 for an optimal configuration is given as follows:

$$[\rho]_{n_\star} = a\alpha^{1/4} m^{-183/370} N^{81/74} \tag{A14}$$

e. **Doubling force.** The extrapolated Hookean force associated with doubling the length of chromosomes is an intensive quantity that can be measured experimentally [19, 43], and which we define within our model as: $f_0 = d(\partial^2 F/\partial d^2)$. For an optimal configuration, we have the following for the doubling force.

$$[f_0]_{n_\star} = (k_B T/a)\alpha^{5/4} m^{-267/370} N^{9/74} \tag{A15}$$

f. **Entropic repulsion between sister chromatids.** The origin of entropic repulsion between the sister chromatid arms is the high osmotic pressure developed in the volume where the sister chromatids overlap. The repulsive force may be computed from the net osmotic pressure over the cross-sectional area of overlap between the intertwined sister chromosomes, $\approx RL'$.

$$f_{rep} = (k_B T/a^3)\langle\varphi\rangle^{9/4} L'R = (k_B T/a)\alpha^{1/2} N^{20/89} \tag{A16}$$

Note that the repulsive force is ≈ 10 pN for monovalent optimal loops of human chromosomes, which drives physical segregation of the intertwined sister chromosomes, a result of the polymer brush morphology of the sister chromatids.

g. **Elastic modulus.** The elastic moduli of chromosomes may be obtained from the average volume fraction of nucleosome monomers inside the cylindrical brush in the following manner [1].

$$E = (k_B T/a^3)\langle\varphi\rangle^{9/4} = (k_B T/a^3)(\alpha/\alpha_{max})^{9/4} \tag{A17}$$

where $k_B T/a^3 \approx 4$ kPa, is the maximum elastic modulus of chromosomes in the limit of the core spanning the entire chromosome.

Metaphase chromosomes of higher eukaryotes are known to have an elastic modulus $E_{meta} \approx 1$ kPa [41]. The value of valency required to generate E_{meta} scales with the total chromosome length, and is given by $\alpha_\star = (0.5)N^{40/89}$. Note that $\alpha_\star$ corresponds to a completely stretched backbone configuration ($m = m_\star$).

- *Prophase limit (fully stretched backbone)*:
  In case of a fully stretched backbone, i.e., $m = m_\star$, the brush becomes stiffer and the above scalings slightly change:

$$[L]_{(n_\star,m_\star)} = aN^{39/89} \tag{A18}$$
$$[R]_{(n_\star,m_\star)} = a\alpha^{-1/2} N^{45/89} \tag{A19}$$
$$[r_0]_{(n_\star,m_\star)} = a\alpha N^{-15/89} \tag{A20}$$
$$[\rho]_{(n_\star,m_\star)} = a\alpha^{1/4} N^{90/89} \tag{A21}$$
$$[f_0]_{(n_\star,m_\star)} = (k_B T/a)\alpha^{5/4} \tag{A22}$$

- *Metaphase limit (highly branched loops)*:
  In metaphase, the valency $\alpha = \alpha_\star = N^{40/89}$ makes the brush even more stiff and compact and further modifies the scaling:

$$[R]_{(n_\star,m_\star,\alpha_\star)} = aN^{25/89} \tag{A23}$$
$$[r_0]_{(n_\star,m_\star,\alpha_\star)} = aN^{25/89} \tag{A24}$$
$$[\rho]_{(n_\star,m_\star,\alpha_\star)} = aN^{100/89} \tag{A25}$$
$$[f_0]_{(n_\star,m_\star,\alpha_\star)} = (k_B T/a)N^{50/89} \tag{A26}$$

3. Confined solution of chromosomes

We model the nuclear confinement of chromosomes by defining an average volume fraction of the confined genome ϕ, which introduces a correlation length associated with the confinement volume fraction.

$$\phi = \mathcal{G}a^3/V = kNa^3/V \tag{A27}$$

where $\mathcal{G}$ and N are, respectively, the total number of monomers in the genome and the chromosome; and k is the total number of chromosomes or the karyotype of the cell: $\mathcal{G} = kN$. The volume of the nucleus is denoted by V [Table II]. Note that chromosomes inside nuclear confinement are expected to have a high degree of overlap: $kR_F(N)^3 \gg V$.

*a. **Entanglements in confinement.*** We estimate inter-chromosome entanglement from the number of nearby contacts between different chromosomes. Since the semidilute solution of chromosomes may be viewed as a closely packed system of blobs, the total number of inter-blob collisions, which scales with the total number of blobs, gives the level of entanglement in the system.

The correlation length in confinement ξ_c, scales with g_c, the number of chromosome monomers in confinement: $\xi_c = \rho^{2/5}(\rho^2 R)^{1/5}g_c^{3/5}$ [1]. Note that the volume of each cylindrical brush monomer is ρR^2, and the excluded volume is $\rho^2 R$. We consider a steady state ensemble, as a result, the number density of chromosome monomers in the confined volume is uniform:

$$\frac{N'}{V} = \frac{g_c}{\xi_c^3} \quad \Rightarrow \xi_c = a\phi^{-3/4}\left(\frac{R_F(N)}{R_F(N')}\right)^{5/4} \tag{A28}$$

where $R_F(N') = \rho^{2/5}(\rho^2 R)^{1/5}(N')^{3/5}$, is the equilibrium end-to-end distance of the chromosome monomer. The total number of confinement blobs, given as follows,

$$N_{blobs} = N'/g_c = N\phi^{5/4}\left(\frac{R_F(N')}{R_F(N)}\right)^{15/4} \tag{A29}$$

scales positively with the chromatin volume fraction ϕ [5]. This indicates a higher entanglement between chromosomes when the average nucleosome concentration in the nucleus is higher.

The level of inter-chromosome entanglement, which we denote by average catenation-squared $\langle \mathrm{Ca}^2 \rangle$, since every catenation irrespective of their sign contribute to entanglement, a consequence of fluctuating topology, scales with the number of blobs, we get the following for inter-chromosomal entanglements per chromosome.

$$\langle \mathrm{Ca}^2 \rangle = N_{blobs}/N_e = \langle \mathrm{Ca}^2 \rangle_0 \left(\frac{R_F(N')}{R_F(N)}\right)^{15/4} \tag{A30}$$

where $\langle \mathrm{Ca}^2 \rangle_0 = N\phi^{5/4}/N_e$, is the level of entanglement in a semidilute chromatin solution, i.e., in the unextruded state; and $N_e \approx 100$ is the entanglement number which is a constant of proportionality [5, 40, 77].

The level of entanglement has a strong positive power law with the end-to-end distance of the cylindrical brush chromosomes. For the optimal configuration, the chromosome contour length L', which is also the same as the end-to-end distance due to its semiflexible nature ($R_F(N') \approx L'$), is minimized leading to a minimization of entanglements for optimal loops: $\langle \mathrm{Ca}^2 \rangle \sim (L')^{15/4} \Rightarrow (\partial \langle \mathrm{Ca}^2 \rangle/\partial n)_{n_\star} = 0$.

Inter-chromosome entanglements per chromosome, for an optimal configuration is given by,

$$[\langle \mathrm{Ca}^2 \rangle]_{n_\star} = \langle \mathrm{Ca}^2 \rangle_0 (m/N)^{27/37} \tag{A31}$$

and in the fully stretched backbone case,

$$[\langle \mathrm{Ca}^2 \rangle]_{(n_\star, m_\star)} = \langle \mathrm{Ca}^2 \rangle_0 N^{-54/89} \tag{A32}$$

4. Bacterial chromosomes: cylindrical DNA monomers

Bacteria does not have nucleosomes, however, bacterial DNA is covered with various DNA binding proteins that slightly increases the thickness of the DNA cross-section from its bare cross section of ≈ 2 nm. We consider bacterial DNA to be a polymer of cylindrical monomers of height $a = 50$ nm, which is the persistence length of bare DNA, and diameter $b = 4$ nm corresponding to protein-bound DNA. We define an asymmetry parameter $\lambda = a/b \approx 10$ and

organism	genome size (Mb)	karyotype k	chromosome size (Mb)	N	nuclear volume V (μm^3)	volume fraction ϕ
Lily (*L. longiflorum*)	97000	24	4000	2×10^7	1347 [78]	0.36
Newt (*N. viridescens*)	95000	24	4000	2×10^7	4174 [79]	0.11
Human (*H. sapiens*)	6000	46	130	6.5×10^5	300 [79, 80]	0.1
Mouse (*M. musculus*)	5600	40	140	7×10^5	400 [79, 81, 82]	0.07
Toad (*X. laevis*)	5400	46	120	6×10^5	307 [79]	0.09
Chicken (*G. gallus*)	2200	78	28	1.4×10^5	210 [79]	0.05
Fly (*D. melanogaster*)	280	8	35	1.7×10^5	78 [79]	0.02
Thale cress (*A. thaliana*)	240	10	24	1.2×10^5	70 [83, 84]	0.02
Nematode (*C. elegans*)	200	12	17	8.3×10^4	200 [85, 86]	0.005
Fission yeast (*S. pombe*)	25	6	4	2.1×10^4	12 [87–89]	0.01
Budding yeast (*S. cerevisiae*)	25	32	0.8	3.9×10^3	3 [79, 90, 91]	0.04
Bacteria (*E. coli*)	9.2	2	4.6	2.3×10^4	2 [92]	0.02

TABLE II. Genome size in a diploid nuclei in Mega-base pair units (1 Mb=10^3 kb) and karyotype k are used to obtain the average chromosome length N. The number of monomers or nucleosomes may be obtained by dividing the chromosome length in Mb by ≈ 0.2 kb corresponding to one nucleosome. Nuclear volumes of various organisms V are used to compute the average volume fraction of chromatin inside nuclear confinement: $\phi = kNa^3/V$, where $a \approx 10$ nm is the nucleosome diameter. Note, bacterial chromosomes are made up of cylindrical segments of length $a \approx 50$ nm and width $b \approx 5$ nm (corresponding to protein-bound DNA), where the volume fraction is computed as $\phi = kNab^2/V$.

express our results in terms of a and λ. We will see that the power law scaling associated with λ is small and only provides a prefactor correction that may be neglected in our scaling study.

The total volume occupied by the genomic elements in bacteria is $\approx Nab^2$, and the equilibrium end-to-end distance of an unconfined bacterial genome is given as follows [1]:

$$R_F(N) = a^{2/5}(a^2b)^{1/5}N^{3/5} = a\lambda^{-1/5}N^{3/5} \tag{A33}$$

Following the steps outlined above Eq. A2 to Eq. A7, we obtain for interloop distance:

$$d = a\lambda^{-1/5}m^{12/25}n^{3/25} \tag{A34}$$

Note that λ dependence drop out of L' minimization, making $n_\star$ independent on the aspect ratio parameter. However, the net axial distance of the brush polymer for optimal configuration has a weak λ dependence:

$$L' = a\lambda^{-1/5}m^{36/185}N^{15/37} \tag{A35}$$

The level of inter-chromosomal entanglements, however, once again, is independent of the aspect ratio parameter, since the quantity: $L'/R_F(N)$, has no λ dependence, making our discussion for symmetric nucleosomes exactly applicable to bacteria.

[1] P. G. DeGennes, *Scaling Concepts in Physics* (Cornell, Ithaca, NY, 1977).
[2] O. Cuvier and T. Hirano, J. Cell Biol. **160**, 645 (2003).
[3] P. A. Coelho, J. Cell Sci. **116**, 4763 (2003).
[4] E. Piskadlo, A. Tavares, and R. A. Oliveira, eLife **6**, e26120 (2017).
[5] J. F. Marko, Phys. Rev. E **79**, 051905 (2009).
[6] J. F. Marko, J. Stat. Phys. **142**, 1353 (2011).
[7] E. Alipour and J. F. Marko, Nucl. Acids Res. **40**, 11202 (2012).
[8] A. Goloborodko, J. F. Marko, and L. A. Mirny, Biophys. J. **110**, 2162 (2016).
[9] J. R. Paulson and U. Laemmli, Cell **12**, 817 (1977).
[10] M. P. Marsden and U. K. Laemmli, Cell **17**, 849 (1979).
[11] J. Rattner and C. Lin, Cell **42**, 291 (1985).
[12] F. Benedetti, J. Dorier, Y. Burnier, and A. Stasiak, Nucl. Acids Res. **42**, 2848 (2014).
[13] C. A. Brackley, J. Johnson, D. Michieletto, A. N. Morozov, M. Nicodemi, P. R. Cook, and D. Marenduzzo, Phys. Rev. Lett. **119**, 138101 (2017).
[14] C. A. Miermans and C. P. Broedersz, J. Royal Soc. Interface **15**, 20180495 (2018).

organism	chromosome size (Mb)	chromosome domains and TADs (kb)	metaphase loops (kb)	L' (μm)	R (μm)	f_0 (nN)	E (kPa)
Newt (*N. viridescens*)	4000	–	–	20 [44]	1.6 [44]	1 [44]	0.7 [44]
Pine (*P. taeda*)	1800	–	–	18 [93]	1 [93]	–	–
Grasshopper (*C. parallelus*)	1400	–	–	–	–	–	0.43 [94]
Deer (*M. muntjak*)	750	–	–	11 [95]	0.96 [95]	–	–
Barley (*H. vulgare*)	729	–	–	12 [93]	0.9 [93]	–	–
Toad (*X. laevis*)	150	–	90[96]	5 [44, 96]	0.8 [44]	0.6 [43]	0.4[44]
Mouse (*M. musculus*)	140	350[29], 880 [97]	50 [98]	–	–	–	–
Human (*H. sapiens*)	130	200 [32], 880 [97]	50 [9]	4.3 [95]	0.88 [95]	0.25 [19]	0.42[19]
Zebrafish (*D.rerio*)	78	500 [99]	–	–	–	–	–
Fly (*D. melanogaster*)	35	60 [97, 100, 101]	–	3.9 [93]	0.4 [93]	–	–
Rice (*O. sativa*)	31	45[102], 487[103]	–	2.5 [93]	0.3 [93]	–	–
Chicken (*G. gallus*)	28	80 [25]	–	–	–	–	–
Roundworm (*C. elegans*)	17	1000 [104]	–	–	–	–	–
Fission yeast (*S. pombe*)	4	50 [105, 106], 80 [107, 108]	–	–	–	–	–
Budding yeast (*S. cerevisiae*)	0.8	100[109], 200 [110]	–	1 [111]	0.5 [111]	–	–
Bacteria (*E. coli*)	4.6	170 [112]	–	2 [50]	–	–	–

TABLE III. Chromosome loop sizes for various organisms corresponding to interphase (TAD) and mitosis are tabulated. Experimental values for the structure and mechanical properties: chromosome axial contour length L', width R, doubling force f_0 in nano-Newton units (nN), and elastic modulus or Young's modulus E in kilo-Pascal units (kPa). Note, the elastic modulus reported in Ref. [94] is for migratory grasshopper (*M. sanguinipes*) chromosomes, however, due to lack of genomic data on *M. sanguinipes*, we use the genomic data for meadow grasshopper (*C. parallelus*).

[15] B. Zhang and P. G. Wolynes, Phys. Rev. Lett. **116**, 248101 (2016).

[16] M. Di Pierro, B. Zhang, E. L. Aiden, P. G. Wolynes, and J. N. Onuchic, Proc. Natl. Acad. Sci. U.S.A. **113**, 12168 (2016).

[17] T. Ono, A. Losada, M. Hirano, M. P. Myers, A. F. Neuwald, and T. Hirano, Cell **115**, 109 (2003).

[18] T. Hirota, D. Gerlich, B. Koch, J. Ellenberg, and J.-m. Peters, J. Cell Sci. **117**, 6435 (2004).

[19] M. Sun, R. Kawamura, and J. F. Marko, Phys. Biol **8**, 1 (2011).

[20] G. Wutz, C. Várnai, K. Nagasaka, D. A. Cisneros, R. R. Stocsits, W. Tang, S. Schoenfelder, G. Jessberger, M. Muhar, M. J. Hossain, N. Walther, B. Koch, M. Kueblbeck, J. Ellenberg, J. Zuber, P. Fraser, and J.-m. Peters, EMBO J. **36**, 3573 (2017).

[21] T. Ono, C. Sakamoto, M. Nakao, N. Saitoh, and T. Hirano, Mol. Biol. Cell **28**, 2875 (2017).

[22] L. F. Rosin, S. C. Nguyen, and E. F. Joyce, PLoS Genet. **14**, 1 (2018).

[23] N. Walther, M. J. Hossain, A. Z. Politi, B. Koch, M. Kueblbeck, Ø. Ødegård-Fougner, M. Lampe, and J. Ellenberg, J. Cell Biol. (2018), 10.1083/jcb.201801048.

[24] L. Vian, A. Pękowska, S. S. Rao, K. R. Kieffer-Kwon, S. Jung, L. Baranello, S. C. Huang, L. El Khattabi, M. Dose, N. Pruett, A. L. Sanborn, A. Canela, Y. Maman, A. Oksanen, W. Resch, X. Li, B. Lee, A. L. Kovalchuk, Z. Tang, S. Nelson, M. Di Pierro, R. R. Cheng, I. Machol, B. G. St Hilaire, N. C. Durand, M. S. Shamim, E. K. Stamenova, J. N. Onuchic, Y. Ruan, A. Nussenzweig, D. Levens, E. L. Aiden, and R. Casellas, Cell **173**, 1165 (2018).

[25] J. H. Gibcus, K. Samejima, A. Goloborodko, I. Samejima, N. Naumova, J. Nuebler, M. Kanemaki, L. Xie, J. R. Paulson, W. C. Earnshaw, L. A. Mirny, and J. Dekker, Science **6135** (2018), 10.1126/science.aao6135.

[26] T. Terakawa, S. Bisht, J. M. Eeftens, C. Dekker, C. H. Haering, and E. C. Greene, Science **358**, 672–676 (2017).

[27] A. M. Ganji, I. A. Shaltiel, S. Bisht, E. Kim, A. Kalichava, C. H. Haering, and C. Dekker, Science **7831**, 1 (2018).

[28] E. Lieberman-aiden, N. L. V. Berkum, L. Williams, M. Imakaev, T. Ragoczy, A. Telling, I. Amit, B. R. Lajoie, P. J. Sabo, M. O. Dorschner, R. Sandstrom, B. Bernstein, M. A. Bender, M. Groudine, A. Gnirke, J. Stamatoyannopoulos, and L. A. Mirny, Science **33292**, 289 (2009).

[29] E. P. Nora, B. R. Lajoie, E. G. Schulz, L. Giorgetti, I. Okamoto, N. Servant, and E. . . . Heard, Nature **485**, 381–385 (2012).

[30] T. Sexton, E. Yaffe, E. Kenigsberg, F. Bantignies, B. Leblanc, M. Hoichman, H. Parrinello, A. Tanay, and G. Cavalli, Cell **148**, 458–472 (2012).

[31] N. Naumova, M. Imakaev, G. Fudenberg, Y. Zhan, B. R. Lajoie, L. A. Mirny, and J. Dekker, Science **342**, 948 (2014).

[32] S. S. P. Rao, M. H. Huntley, N. C. Durand, E. K. Stamenova, I. D. Bochkov, J. T. Robinson, A. L. Sanborn, I. Machol, A. D. Omer, E. S. Lander, and E. Lieberman-Aiden, Cell **159**, 1665 (2014).

[33] A. L. Sanborn, S. S. P. Rao, S. C. Huang, N. C. Durand, M. H. Huntley, A. I. Jewett, and E. L. . . . Aiden, Proc. Natl. Acad. Sci. U.S.A. **112**, E6456–E6465 (2015).

[34] J. F. Marko and E. D. Siggia, Mol. Biol. Cell **8**, 22217 (1997).

[35] A. Goloborodko, M. V. Imakaev, J. F. Marko, and L. A. Mirny, eLife **e14864** (2016), 10.7554/eLife.14864.

[36] S. Panyukov, E. B. Zhulina, S. S. Sheiko, G. C. Randall, J. Brock, and M. Rubinstein, J Phys. Chem. B **113**, 3750 (2009).

[37] H. Li and T. A. Witten, Macromolecules **27**, 449 (1994).

[38] L. Feuz, F. A. M. Leermakers, M. Textor, and O. Borisov, Macromolecules **38**, 8891 (2005).

[39] M. Daoud and J. P. Cotton, Journal de Physique **43**, 531 (1982).

[40] A. Rosa and R. Everaers, PLoS Comp. Biol. **4**, e1000153 (2008).

[41] J. F. Marko, Chromosome Res. **16**, 469 (2008).

[42] S. Sazer, M. Lynch, and D. Needleman, Curr. Biol. **24**, R1099–R1103 (2014).

[43] B. Houchmandzadeh, J. F. Marko, D. Chatenay, and A. Libchaber, J. Cell Biol. **139**, 1–12 (1997).

[44] M. G. Poirier, S. Eroglu, and J. F. Marko, Mol. Biol. Cell **13**, 2170–2179 (2002).

[45] K. K. Swinger and P. A. Rice, Curr. Opin. Struct. Biol. **14**, 28 (2004).

[46] V. V. Rybenkov, V. Herrera, Z. M. Petrushenko, and H. Zhao, Journal of Molecular Microbiology and Biotechnology **24**, 371–383 (2014).

[47] J. F. Marko and E. D. Siggia, Macromolecules **28**, 8759 (1995).

[48] J. F. Marko, Phys. Rev. E **76**, 021926 (2007).

[49] S. Jun and B. Mulder, Proc. Natl. Acad. Sci. U.S.A. **103**, 12388 (2006).

[50] X. Wang, P. M. Llopis, and D. Z. Rudner, Nat. Rev. Genet. **14**, 191 (2013).

[51] J. Pelletier, K. Halvorsen, B.-Y. Ha, R. Paparcone, S. J. Sandler, C. L. Woldringh, W. P. Wong, and S. Jun, Proc. Natl. Acad. Sci. U.S.A. **109**, E2649 (2012).

[52] M. Sun, R. Biggs, J. Hornick, and J. F. Marko, Chromosome Res. **26**, 277 (2018).

[53] T. R. Strick, T. Kawaguchi, and T. Hirano, Curr. Biol. **14**, 874 (2004).

[54] M. Sun, T. Nishino, and J. F. Marko, Nucl. Acids Res. **41**, 6149 (2013).

[55] R. A. Keenholtz, T. Dhanaraman, R. Palou, J. Yu, D. D'Amours, and J. F. Marko, Sci. Rep. **7** (2017), 10.1038/s41598-017-14701-5.

[56] J. M. Eeftens, S. Bisht, J. Kerssemakers, M. Kschonsak, and C. H. Haering, EMBO J. **36**, 3448 (2017).

[57] J. F. Marko, P. D. L. Rios, A. Barducci, and S. Gruber, bioRxiv (2018), 10.1101/325373.

[58] R. T. Johnson and P. N. Rao, Nature **226**, 717 (1970).

[59] S.-i. Matsui, H. Yoshida, H. Weinfeld, and A. Sandberg, J. Cell Biol. **54**, 120 (1973).

[60] L. J. Burke, R. Zhang, M. Bartkuhn, V. K. Tiwari, G. Tavoosidana, S. Kurukuti, C. Weth, J. Leers, N. Galjart, R. Ohlsson, and R. Renkawitz, EMBO J. **24**, 3291 (2005).

[61] W. Shen, D. Wang, B. Ye, M. Shi, Y. Zhang, and Z. Zhao, Biol. Res. , 1 (2015).

[62] A. T. Sumner, Chromosoma Res. **100**, 410 (1991).

[63] K. Shintomi and T. Hirano, Gen. Dev. **25**, 1464 (2011).

[64] L. C. Green, P. Kalitsis, T. M. Chang, M. Cipetic, J. H. Kim, O. Marshall, L. Turnbull, C. B. Whitchurch, P. Vagnarelli, K. Samejima, W. C. Earnshaw, K. H. A. Choo, and D. F. Hudson, J. Cell Sci. **125**, 1591 (2012).

[65] M. Houlard, J. Godwin, J. Metson, J. Lee, and T. Hirano, Nat. Cell Biol. **17**, 771 (2017).

[66] D. Gerlich, T. Hirota, B. Koch, J.-m. Peters, and J. Ellenberg, Curr. Biol. **16**, 333 (2006).

[67] A. Zhiteneva, J. J. Bonfiglio, A. Makarov, T. Colby, P. Vagnarelli, E. C. Schirmer, and W. C. ... Earnshaw, Open Biology **7** (2017), 10.1098/rsob.170076.

[68] C. R. Bauer, T. A. Hartl, and G. Bosco, PLoS Comp. Biol. **8**, 1 (2012).

[69] T. Ono, D. Yamashita, and T. Hirano, J. Cell Biol. **200**, 429 (2013).

[70] J. Lawrimore, P. A. Vasquez, M. R. Falvo, R. M. Taylor, L. Vicci, E. Yeh, G. G. Forest, and K. Bloom, J. Cell Biol. **210**, 553 (2015).

[71] J. Lawrimore, J. K. Aicher, P. Hahn, A. Fulp, B. Kompa, L. Vicci, M. Falvo, R. M. Taylor, and K. Bloom, Mol. Biol. Cell **27**, 153 (2016).

[72] M. Di Pierro, R. R. Cheng, E. Lieberman Aiden, P. G. Wolynes, and J. N. Onuchic, Proc. Natl. Acad. Sci. U.S.A. (2017), 10.1073/pnas.1714980114.

[73] J. Nuebler, G. Fudenberg, M. Imakaev, N. Abdennur, and L. A. Mirny, Proc. Natl. Acad. Sci. U.S.A. **115**, E6697 (2018).

[74] M. Doi and S. F. Edwards, *Theory of Polymer Dynamics* (Oxford Univ. Press, Oxford, 1986).

[75] M. Daoud and P. De Gennes, Journal de Physique **38**, 85 (1977).

[76] P. Pincus, Macromolecules **9**, 386 (1976).

[77] J. D. Halverson, J. Smrek, K. Kremer, and A. Y. Grosberg, Rep. Prog. Phys **77** (2014), 10.1088/0034-4885/77/2/022601.

[78] K. P. Baetcke, A. H. Sparrow, C. H. Nauman, and S. S. Schwemmer, Proc. Natl. Acad. Sci. U.S.A. **58**, 533–540 (1967).

[79] G. Maul and L. Deaven, J. Cell Biol. **73**, 748 (1977).

[80] J. Schwarz-Finsterle, H. Scherthan, A. Huna, P. González, P. Mueller, E. Schmitt, J. Erenpreisa, and M. Hausmann, Mutation Research/Genetic Toxicology and Environmental Mutagenesis **756**, 56 (2013), from DNA Damage to Chromosomal Aberrations.

[81] R. R. Snapp, E. Goveia, L. Peet, N. A. Bouffard, G. J. Badger, and H. M. Langevin, Journal of Anatomy **223**, 255–261 (2013).

[82] D.-H. Kim, B. Li, F. Si, J. M. Phillip, D. Wirtz, and S. X. Sun, J. Cell Sci. **128**, 3375 (2015).

[83] T. A. Dittmer, N. J. Stacey, K. Sugimoto-Shirasu, and E. J. Richards, The Plant Cell **19**, 2793 (2007).

[84] L. Willis, Y. Refahi, R. Wightman, B. Landrein, J. Teles, K. C. Huang, E. M. Meyerowitz, and H. Jönsson, Proc. Natl. Acad. Sci. U.S.A. **113**, E8238 (2016).

[85] Y. Arata, H. Takagi, Y. Sako, and H. Sawa, Frontiers in Physiology **5**, 529 (2014).

[86] S. Uppaluri, S. Weber, and C. Brangwynne, Cell Rep. **17**, 345 (2016).

[87] Y. Gonzalez, K. Meerbrey, J. Chong, Y. Torii, N. N. Padte, and S. Sazer, J. Cell Sci. **122**, 2464 (2009).

[88] A. Takemoto, S. A. Kawashima, J.-J. Li, L. Jeffery, K. Yamatsugu, O. Elemento, and P. Nurse, J. Cell Sci. **129**, 1250

(2016).

[89] F. R. Neumann and P. Nurse, J. Cell Biol. **179**, 593–600 (2007).

[90] R. P. Joyner, J. H. Tang, J. Helenius, E. Dultz, C. Brune, L. J. Holt, and K. ... Weis, eLife **5**, e09376 (2016).

[91] P. Jorgensen, N. P. Edgington, B. L. Schneider, I. Rupeš, M. Tyers, and B. Futcher, Mol. Biol. Cell **18**, 3523–3532 (2007).

[92] H. E. Kubitschek and J. A. Friske, J. Bacteriol. **168**, 1466–1467. (1986).

[93] J. R. Daban, J. Royal Soc. Interface **11** (2014), 10.1098/rsif.2013.1043.

[94] R. B. Nicklas, J. Cell Biol. **97**, 542–548 (1983).

[95] T. D. Allen, E. M. Jack, and C. J. Harrison, *Chromosomes and Chromatin, Vol II (p 54)*, edited by K. W. Adolph (CRC Press, Boca Raton, 1988).

[96] G. Micheli, A. Rosa, C. Lnzzatto, M. T. Carri, A. D. Capoa, F. Pelliccia, C. A. N. C. N. R, U. Roma, L. Sapienza, D. Biologia, R. Iii, D. Biologia, U. Roma, T. Vergata, B. Molecolare, U. Roma, and L. Sapienza, Chromosoma **102**, 478 (1993).

[97] J. R. Dixon, S. Selvaraj, F. Yue, A. Kim, Y. Li, Y. Shen, and B. ... Ren, Nature **485**, 376–380 (2012).

[98] J. Filipski, J. Leblanc, T. Youdale, M. Sikorska, and P. R. Walker, EMBO J. **9**, 1319 (1990).

[99] L. J. Kaaij, R. H. van der Weide, R. F. Ketting, and E. de Wit, Cell Rep. **24**, 1 (2018).

[100] C. Hou, L. Li, Z. S. Qin, and V. G. Corces, Mol. Cell **48**, 471–484 (2012).

[101] F. Ramírez, V. Bhardwaj, L. Arrigoni, K. C. Lam, B. A. Grüning, J. Villaveces, B. Habermann, A. Akhtar, and T. Manke, Nat. Commun. **9** (2018), 10.1038/s41467-017-02525-w.

[102] C. Liu, Y.-J. Cheng, J.-W. Wang, and D. Weigel, Nature Plants **3**, 742 (2017).

[103] Q. Dong, N. Li, X. Li, Z. Yuan, D. Xie, X. Wang, J. Li, Y. Yu, J. Wang, B. Ding, Z. Zhang, C. Li, Y. Bian, A. Zhang, Y. Wu, B. Liu, and L. Gong, Plant J. **94**, 1141 (2018).

[104] E. Crane, Q. Bian, R. P. McCord, B. R. Lajoie, B. S. Wheeler, E. J. Ralston, and B. J. ... Meyer, Nature **523**, 240–244 (2015).

[105] H. Tanizawa, K. D. Kim, O. Iwasaki, and K. Noma, Nat. Struct. Mol. Biol. **24**, 965–976 (2017).

[106] T. Mizuguchi, G. Fudenberg, S. Mehta, J. M. Belton, N. Taneja, H. D. Folco, and S. I. S. ... Grewal, Nature **516**, 432–435 (2014).

[107] Y. Kakui, A. Rabinowitz, D. J. Barry, and F. Uhlmann, Nat. Genet. **49**, 1553 (2017).

[108] K. D. Kim, H. Tanizawa, O. Iwasaki, and K. Noma, Nat. Genet. **48**, 1242–1252 (2016).

[109] C. Nikolaou, Curr. Genet. **64**, 247 (2018).

[110] U. Eser, D. Chandler-Brown, F. Ay, A. F. Straight, Z. Duan, W. S. Noble, and J. M. Skotheim, Proc. Natl. Acad. Sci. U.S.A. **114**, E3061 (2017).

[111] R. Koszul, K. Kim, M. Prentiss, N. Kleckner, and S. Kameoka, Cell **133**, 1188 (2008).

[112] T. B. K. Le, M. V. Imakaev, L. A. Mirny, and M. T. Laub, Science (New York, N.Y.) **342**, 731–734 (2013).